Ray splitting in a class of chaotic triangular step billiards

A. Kohler,* G. H. M. Killesreiter,† and R. Blümel‡
Fakultät für Physik, Universität Freiburg, Hermann-Herder-Straße 3, D-79104 Freiburg, Germany
(Received 12 March 1997)

For a class $\mathcal{T}$ of triangular step billiards (TSBs) we prove analytically the absence of elliptic islands in phase space. There is numerical evidence that TSBs are ergodic, sensitive, and mixing. Thus TSBs are chaotic, although their Kolmogorov-Sinai entropy is zero. We study the quantum implications of ray splitting (RS) in TSBs. The signature of non-Newtonian periodic RS orbits is identified in the Fourier transform of the TSB level density. The RS correction of the Weyl formula is tested in the TSB context. In contrast to the rich structure of split circle wave functions, TSB wave functions, except for the emergence of short-range correlations in the form of scarlets, appear featureless and homogeneous. [S1063-651X(97)06109-6]

PACS number(s): 05.45.+b

I. INTRODUCTION

Ray splitting may occur in all wave systems with sharply defined interfaces. Light rays, e.g., are split into transmitted and reflected rays at the interface between two dielectrica with different index of refraction, and acoustic waves generated by an earthquake experience ray splitting at fault lines. Apart from optics and acoustics ray-splitting (RS) phenomena occur, e.g., in hydrodynamics, microwaves, and quantum mechanics. Thus, ray splitting is universal. Its wave implications, however, have only recently been investigated. Couchman *et al.* [1] studied ray splitting in the context of acoustic and quantum chaos. Prange *et al.* [2] computed analytically the RS correction to the Weyl formula [3]. Blümel *et al.* [4,5] investigated RS phenomena in a chaotic circular step billiard. They identified the signatures of non-Newtonian RS orbits in the Fourier transform of the scaled level density, thereby demonstrating the importance of periodic non-Newtonian RS orbits for trace formulas pertaining to RS systems. Recently Sirko *et al.* [6] identified experimentally the signatures of non-Newtonian RS orbits in the resonance spectra of a microwave cavity partially filled with Teflon.

In this paper we study the classical and quantum mechanics of a class $\mathcal{T}$ of triangular step billiards (TSBs). Without the potential step these billiards are pseudointegrable [7]. With the potential step, TSBs are chaotic. We show that the TSB phase-space structure is simpler than the mixed phase space of circular step billiards. There are, e.g., no elliptic islands in the phase space of TSBs. We present a classical analysis of $\mathcal{T}$ in Section II. The quantum mechanics of $\mathcal{T}$ is investigated in Sec. III. Section IV summarizes our findings and concludes the paper.

II. CLASSICAL MECHANICS

A TSB consists of a mass point m bouncing inside a triangular enclosure divided into two domains by an RS boundary R (see Fig. 1). A typical TSB is shown in Fig. 1(a). One of the two domains is kept at potential $V=0$, while the other is kept at $V=V_0>0$. Thus, a discontinuous step of the potential occurs along R, which, in a quantum treatment of the TSB, gives rise to RS phenomena analyzed in detail in Sec. III. While a complete analysis of arbitrary TSBs is possible, it is not necessary for our purposes. In this paper we investigate a restricted set $\mathcal{T}$ of TSBs defined in Sec. II A. In Sec. II B we introduce the bouncing rule, which states that an orbit started anywhere inside a TSB$\in\mathcal{T}$ has to reach the RS boundary R after a finite number of bounces with the sides of the TSB. The bouncing rule is purely geometric. In Section II C we extend the bouncing rule to the crossing rule, which states that, given a certain condition, any orbit in a TSB$\in\mathcal{T}$ actually has to cross R after a finite number of ''trials.'' The

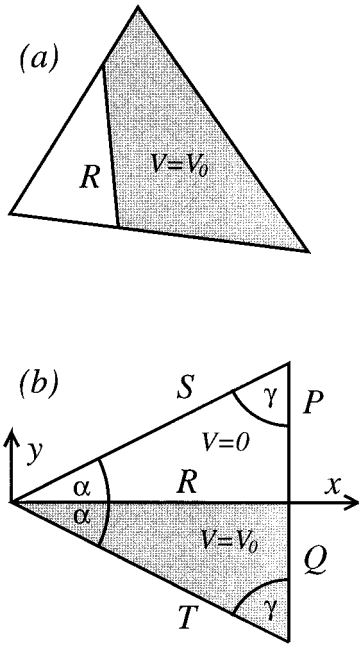

FIG. 1. Triangular step billiards (TSBs). (a) A general TSB. The ray-splitting boundary R separates the two domains of the billiard with $V=0$ (the white region inside the TSB) and $V=V_0>0$ (the grey region inside the TSB). (b) A special TSB$\in\mathcal{T}$, the class of RS billiards considered in this paper.

*Electronic address: ako@phyc1.physik.uni-freiburg.de
†Electronic address: killes@phyc1.physik.uni-freiburg.de
‡Electronic address: blumel@phyc1.physik.uni-freiburg.de

crossing rule is a dynamic rule. Because of the possibility of total classical internal reflection discussed in Sec. II A, the bouncing rule does not imply the crossing rule. In Sec. II D we introduce a symbolic dynamics for coding TSB trajectories. In Sec. II E we present Newtonian and non-Newtonian periodic TSB orbits. In Sec. II F we construct the Poincaré mapping of the TSB. Here we make decisive use of the crossing rule when choosing R as our surface of section. In Sec. II G we prove the absence of elliptic islands of any order in the TSB phase space. Visual inspection of the TSB surface of section corroborated by a more detailed numerical analysis presented in Sec. II H indicates that TSBs are ergodic, sensitive, and mixing. Thus TSBs are chaotic, alas with zero Kolmogorov-Sinai (KS) entropy.

A. Definitions

A typical member of the restricted set $\mathcal{T}$ of TSBs considered in this paper is shown in Fig. 1(b). It is defined by the following requirements. (i) Only isosceles triangles are considered. (ii) The base angle γ is restricted to the range $\pi/3<\gamma<\pi/2$. (iii) The RS boundary R is orthogonal to the baseline of the TSB and divides the TSB into two domains of equal size. The RS boundary is assumed to be rectilinear throughout this paper, although curved RS boundaries are certainly interesting and deserve further investigation. The sides of a given TSB$\in\mathcal{T}$ are labeled with the letters S, P, Q, and T. Throughout this paper we choose units such that the length of the RS boundary is 1, $m=1/2$ and $\hbar=1$. Thus, according to Fig. 1(b), $R=\{(x,y=0):0\leqslant x\leqslant 1\}$. Although according to their definition the letters P, Q, R, S, and T denote point sets, we will also use them in Sec. II D as the symbols of a symbolic dynamics for the TSB. This is possible since a confusion between point sets and symbols of an alphabet seems unlikely. Often we will have to focus on a specific TSB$\in\mathcal{T}$. We choose quite arbitrarily the TSB with $\gamma=7\pi/20$ and denote it by TSB$_0(V_0)$. TSB$_0(V_0)$ is a rational triangle, pseudointegrable for $V_0=0$ [7]. For $V_0\neq 0$ this property is lost and TSB$_0(V_0>0)$ is chaotic (see Sec. II H). Denoting the interior of the TSB by Δ, we define the upper and lower parts of the TSB according to

$$\Delta_u=\{(x,y)\in\Delta:y>0\},$$
$$\Delta_l=\{(x,y)\in\Delta:y<0\}, \tag{1}$$

respectively. The potential experienced by the particle bouncing inside the TSB is given by

$$V(x,y)=\begin{cases}0, & (x,y)\in\Delta_u\\ V_0, & (x,y)\in\Delta_l\\ \infty, & (x,y)\notin\Delta.\end{cases} \tag{2}$$

In the units defined above, the classical Hamiltonian function is given by

$$H=E=p_x^2+p_y^2+V(x,y). \tag{3}$$

In either part of the TSB, Δ_u or Δ_l, the motion of the particle is free [$\vec{\nabla}V(x,y)=0$ in Δ_u,Δ_l] with specular reflections at the outer boundaries of the TSB. The refractive transmission through R (see Fig. 2) is found by minimizing the action. This results in Snell's law of refraction. We note that because of $\nabla_x V=0$ on R we have $p_x=p_x'$. From Eq. (3) it follows immediately that

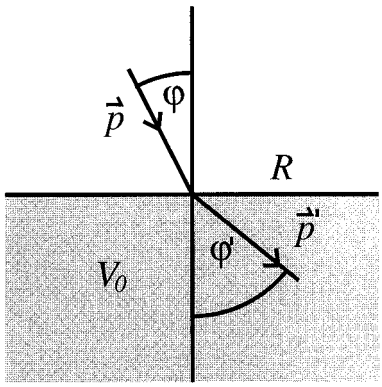

FIG. 2. Refraction of a classical orbit with momentum $\vec{p}$ when crossing from a region with potential $V=0$ through a ray-splitting boundary R into a region with $V=V_0>0$. The relation between the incident angle φ and the final angle φ' is given by Snell's law.

$$\sqrt{E}\sin(\varphi)=\sqrt{E-V_0}\sin(\varphi'). \tag{4}$$

Defining

$$\eta=V_0/E \tag{5}$$

and

$$\kappa=\sqrt{1-\eta}, \tag{6}$$

Snell's law (4) becomes

$$\sin(\varphi)=\kappa\sin(\varphi'). \tag{7}$$

If the particle originates in Δ_l, it is transmitted through R according to Eq. (4) no matter what its incident angle. Depending on its incident angle a particle orginating in Δ_u is either transmitted according to Eq. (4), or it is specularly reflected at R and thrown back into Δ_u. This latter case is called classical internal reflection. It occurs whenever $\varphi>\varphi_c$, where φ_c is the critical angle given by

$$\sin(\varphi_c)=\kappa. \tag{8}$$

B. Bouncing rule

In this section we prove the bouncing rule for TSBs$\in\mathcal{T}$: a trajectory started anywhere in Δ reaches R after $N\leqslant 3$ bounces. First we focus on a trajectory started in Δ_u. There are three possibilities for its orbit. (i) The trajectory bounces off P, (ii) the trajectory bounces off S, (iii) it reaches R. There is nothing to be proved in case (iii). Case (i) and case (ii) have to be considered further. First we focus on case (i). There are two ways of following the itinerary of a trajectory. Either we plot its zigzag path within Δ_u, or we represent it as a straight line in the plane reflecting the triangle at the side of impact. We choose the latter way. The subsequent reflections relevant to case (i) are shown in Fig. 3(a). The diagram was drawn for the limiting angle of TSBs in $\mathcal{T}$, $\gamma=\pi/3$. Drawing a straight line through an arbitrarily chosen point in

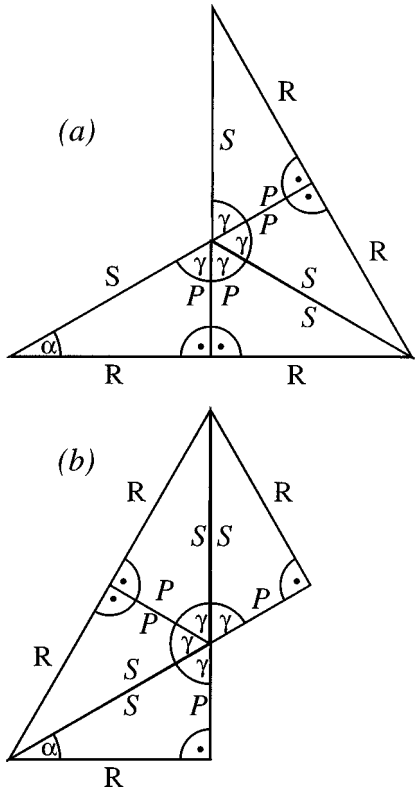

FIG. 3. Replicas of Δ_u of a TSB for proving the bouncing rule. (a) The first encounter of a trajectory started in Δ_u is with the side P of the TSB. (b) The first encounter is with the side S.

Δ_u and an arbitrary point on P we see that for $\gamma > \pi/3$ the straight line intersects with a replica of R after at most $N=3$ intersections with replicas of P or S. This proves the bouncing rule for case (i). The relevant diagram for case (ii) is shown in Fig. 3(b). Again it is obvious that $N \leqslant 3$. This concludes the proof of the bouncing rule for Δ_u. The proof for Δ_l runs along identical lines, thus proving the bouncing rule for Δ.

C. Crossing criterion and crossing rules

Because of the bouncing rule proved in Sec. II B an orbit started anywhere in Δ will reach R after no more than three bounces with the outer boundaries of the TSB. But because of the possibility of classical internal reflection, reaching R does not imply crossing R. Only if the trajectory originates in Δ_l does reaching R actually imply crossing R into Δ_u. For this case we formulate the following crossing rule: a trajectory started in Δ_l will cross R into Δ_u after no more than three bounces with the sides of Δ. It is impossible to formulate a similar rule for Δ_u. In fact, for sufficiently large V_0 there is always at least one orbit forever confined to Δ_u. However, complete deconfinement of trajectories is achieved if the following crossing criterion is fulfilled: $\varphi_c > \alpha$. In order to prove it we consider the following case: a trajectory is internally reflected in x_0 with $\varphi_0 > \varphi_c$ (see Fig. 4). We follow this trajectory to the left. The trajectory hits R again in x_1 with incident angle φ_1. If the momentum in the x direction is positive in x_1 the trajectory will cross the RS boundary, because in this case $\varphi_1 < \alpha < \varphi_c$. If the momentum in the x direction is negative in x_1, $\varphi_1 = \varphi_0 - 2\alpha$. There are

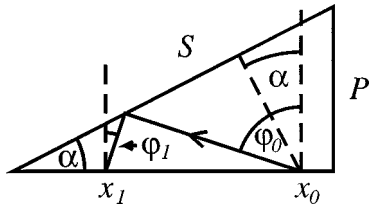

FIG. 4. A trajectory, internally reflected in x_0 with angle φ_0 continues to the left to reach R in x_1 with angle φ_1.

three possible cases. (i) $\varphi_1 > \varphi_c$, (ii) $\varphi_1 = \varphi_c$, and (iii) $\varphi_1 < \varphi_c$. In the third case the trajectory crosses R. In the second case, technically, the trajectory crosses too. After crossing it runs parallel to R in Δ_l at a distance $\epsilon \to 0$ from R and corresponds to a ''lateral ray'' [4]. Lateral rays are not considered further in this paper. In the first case, $\varphi_1 < \varphi_0$, but the trajectory is again internally reflected. Repeating the above procedure, the trajectory will continue to the left. After a finite number n of bounces we have $\varphi_n = \varphi_0 - 2n\alpha < \varphi_c$ and the trajectory crosses R. If the trajectory emerges at x_0 to the right with φ_0 the situation does not change, since after a finite number of internal reflections the particle encounters the corner cube spanned by R and P and reverses its momentum in x direction. From this point on, the above proof applies. Given the crossing criterion this proves the crossing rule in Δ. Along the same lines it is possible to prove that a particle bouncing inside TSB_0 has to cross R after at most one total internal reflection.

D. Symbolic dynamics

We code trajectories of the TSB according to their encounters with R or the sides of Δ, respectively. Therefore the alphabet of a possible symbolic dynamics for the TSB consisits of the set of letters $\{P,Q,R,S,T\}$. Every time a trajectory is reflected at R its symbol string aquires the new letter ''R.'' If it crosses R, no new letter is added to the symbol string. The symbolic description is especially useful for labeling periodic orbits. It is sufficient to label any possible orbit of the TSB. However, not all possible symbol strings correspond to TSB orbits. Grammatical restrictions apply. The simplest grammatical rules are summarized in Table I. We see that repetitions of letters such as SS,PP,TT,QQ,RR are forbidden. Sequences with PQ and QP are not possible either, because a transmission through R cannot change the sign of the momentum in the p_x direction. Because internal reflection is only possible in Δ_u, combinations such as QR,TR,RQ,RT are not allowed. Besides these simple rules there are more complicated grammar

TABLE I. The Markov matrix with the simplest grammar rules for TSBs.

	S	P	T	Q	R
S	0	1	1	1	1
P	1	0	1	0	1
T	1	1	0	1	0
Q	1	0	1	0	0
R	1	1	0	0	0

rules. The sequences RPT,TPT,RPR,TPR do not exist because a bounce at P with positive momentum in the y direction is always followed by a bounce at S. A similar argument shows that SQS is forbidden. Apart from the grammar rules there are parameter dependent pruning rules. But their discussion is not needed for the purposes of this paper.

E. Periodic orbits

There are two major types of periodic orbits in TSBs: Newtonian and non-Newtonian. We label Newtonian orbits with capital letters, non-Newtonian (NN) orbits with lower case letters. Three examples of short Newtonian orbits are shown in Fig. 5. Among other periodic orbits they are listed in Table II together with their symbolic codes and stability properties. We note that the Newtonian orbits $A1$ and $C1$ in Fig. 5 exist over a large interval of V_0 values. The orbit $B1$, however, exists only for a very specific value of V_0, which depends on γ. We will return to this observation in Sec. III D. Apart from NN orbits discussed below the Newtonian orbits are a major ingredient for predicting the quantum level density of the TSB on the basis of the modified Gutzwiller trace formula suggested in [1]. Many more periodic orbits than those listed in Table II are necessary for a proper check of the modified Gutzwiller trace formula. A possible method for finding them is the one studied in [8] and already successfully applied in [9]. In this paper, however, we are content with identifying short Newtonian orbits in the Fourier transform of the TSB level density (see Sec. III D).

NN orbits are orbits that are reflected at R where, according to Newtonian mechanics, they should have been transmitted. Every time the trajectory hits the RS boundary originating in Δ_l, or in Δ_u with $\varphi<\varphi_c$, it ''decides'' whether to cross or to turn around on the basis of the quantum reflection coefficients. This implies a loss of determinism, a feature that contrasts with Newtonian mechanics. Nevertheless these orbits are important for the quantum spectrum. Three series of NN orbits are shown in Fig. 6, ordered according to increasing action of their first member. Initial conditions that generate the an series displayed in the first row of Fig. 6 are $x_n=1$, $p_{xn}=-\sqrt{E-V_0}\cos(\pi/2-n\alpha)$, $p_{yn}<0$, $n=1,2,\ldots$. Another series of NN orbits, the bn series, is shown in the second row of Fig. 6. This series is topologically the same as the an series, but the action of the orbits differs by a factor $1/\sqrt{E-V_0}$. Initial conditions that generate the bn series are $x_n=1$, $p_{xn}=-\sqrt{E}\cos(\pi/2-n\alpha)$, $p_{yn}>0$. For these simple NN orbits the initial conditions are independent of η. The global dynamics of NN orbits is rather complex. The symbol R can be used for all types of reflection at the RS boundary, i.e., for both internal and NN reflections. In order to apply the method introduced in [8] to NN orbits it is necessary to introduce a classification for the NN orbits such that each class by itself is deterministic. Following an investigation of grammar rules, the method of [8] can be used for each class of NN orbits separately. Because of the simple structure of TSBs, location and shape of many of the periodic TSB orbits can be computed analytically. This is demonstrated in Appendix A where we compute analytically and explicitly all characteristics of the Newtonian orbit $C1$.

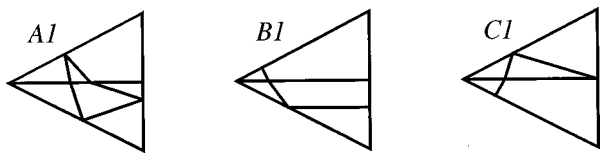

FIG. 5. Short Newtonian orbits of TSB_0.

F. Poincaré map

There are several possibilities for defining a Poincaré surface of section (PSS) for the TSB. We choose R because—as long as the crossing criterion is fullfilled—every orbit in Δ eventually crosses R (see Sec. II C). Concerning the construction of the Poincaré map we record a section point whenever a trajectory crosses R with positive momentum in the y direction. Total internal reflection points do not correspond to section points. As coordinates on the PSS we choose the x coordinate on R and the x component p_x of the momentum in Δ_u. An example of a PSS, the PSS for $TSB_0(1/2)$ at $E=1$, is shown in Fig. 7(a). Because of total internal reflection the maximum of $|p_x|$ is $1/\sqrt{2}$. We generated the PSS by starting a single trajectory with coordinate

TABLE II. The stability Λ_p, the action S_p, and the time T_p for the shortest non-Newtonian and Newtonian periodic orbits for $TSB_0(1/2)$.

Periodic orbit	Alphabet	x	p_x	Λ_p	S_p	T_p
$a1$	RQT	1	−0.321	1	0.642	0.642
$a2$	$RTQRT$	1	−0.572	1	0.932	0.932
$a3$	$TRTQRTR$	1	−0.698	1	1.397	1.397
$b1$	RPS	1	−0.454	1	0.908	0.454
$b2$	$RSPRS$	1	−0.809	1	1.319	0.659
$b3$	$SRSPRSR$	1	−0.988	1	1.975	0.988
$c1$	$TRQTQR$	$x\in(0.74,1)$	−0.321	1	1.284	1.284
$d1$	$SRPSPR$	$x\in(0.74,1)$	−0.454	1	1.816	0.908
$A1$	SQT	0.469	−0.208	−2.243	1.338	1.083
$A1$	STQ	0.617	−0.669	−2.243	1.338	1.083
$B1$	$STQ(\eta=0.403)$	$x\in(0,0.630)$	−0.454	+1	1.543	1.219
$C1$	$SRPSTSPRST$	0.314	+0.321	−1	1.910	1.056
$D1$	$SRPSTSPRST$	$x\in(0,0.627)$	+0.321	+1	3.820	2.112

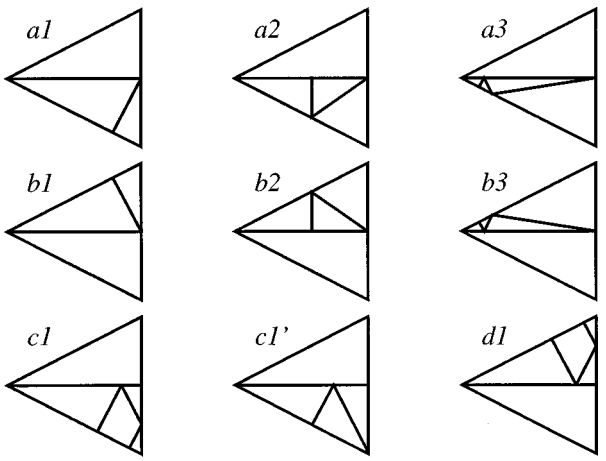

FIG. 6. Short non-Newtonian orbits of TSB_0.

$x=1/2$ and momentum $p_x=1/5$ and iterating it $N=10^6$ times. Visual inspection of the resulting PSS indicates that $TSB_0(1/2)$ is chaotic. The horizontal structure at $p_x\approx 0.32$ is due to a family of marginally stable periodic orbits shown in Fig. 7(b). If the trajectory joins the neighborhood of a marginally stable orbit its local Lyapunov exponent becomes very small and it stays some time in the neighborhood of this marginally stable orbit. This generates the horizontal structure seen in Fig. 7(a). It is proved analytically in Sec. II G that the PSS of a TSB does not contain any elliptic islands. Thus for a larger number of iterations ($N\gg 10^6$) the ''white area'' of the horizontal structure in Fig. 7(a) gradually fills in.

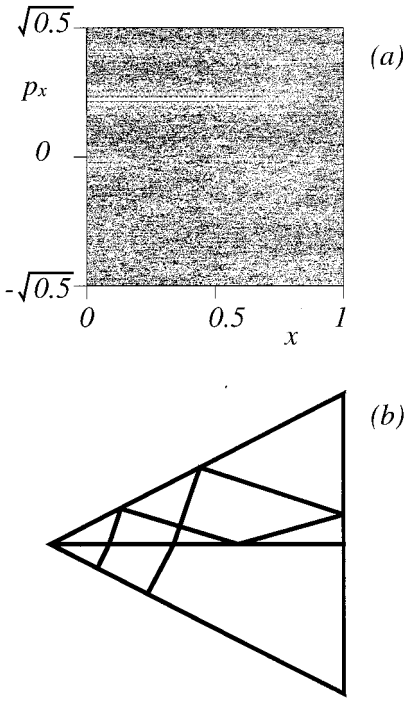

FIG. 7. (a) Poincaré surface of section for $TSB_0(1/2)$ with $E=1$. The motion is chaotic over all of the dynamically accessible phase space. The horizontal structure at $p_x\approx 0.32$ is due to a one-parameter family of marginally stable orbits of the type shown in (b).

It is possible to state the Poincaré map $\mathcal{P}$ of the TSB explicitly with the help of closed analytical expressions. To this end we define the angle β between the trajectory and R according to $p_x=\cos(\beta)$. The Poincaré map is then composed of four parts: $\mathcal{P}=\mathcal{P}_4\mathcal{P}_3\mathcal{P}_2\mathcal{P}_1$. The mapping $\mathcal{P}_1$ traces the trajectories starting on R with positive momentum in the y direction until it hits R again with a momentum which does not allow internal reflection. The possible symbol strings for $\mathcal{P}_1$ and the corresponding mappings for x and β are shown in Table III. The intervals for x and β give the starting points in the PSS that yield the corresponding symbol string. The mapping $\mathcal{P}_2$ represents the transmission through R, which is described by Eq. (7). The mapping $\mathcal{P}_3$ is essentially the same as $\mathcal{P}_1$. The mapping $\mathcal{P}_4$ is again described by Eq. (7). Because of the bouncing and the crossing rules the number of possible symbols in Table III is finite and small. This is the main reason for restricting our investigations to the class $\mathcal{T}$ of TSBs.

G. Absence of elliptic islands

The following proof is not restricted to TSBs. It applies to all polygonal RS billiards and rests on the structure of the stability matrix. The stability matrix of a two-dimensional system is a 4×4 matrix. In Hamiltonian systems it can be reduced to a 2×2 matrix [10]. This is achieved by choosing local coordinates that are, respectively, perpendicular and parallel to the orbit in configuration space and in momentum space. The matrix elements for the coordinates parallel to the orbit are then trivial. The stability matrix in local coordinates then describes the time dependence of an initial displacement of the starting point perpendicular to the orbit (dX,dP) according to

$$\begin{pmatrix} dX' \\ dP' \end{pmatrix} = M \begin{pmatrix} dX \\ dP \end{pmatrix}. \tag{9}$$

For billiards with $V=0$ the stability matrix is derived in [11]. For step billiards there are four different types of motion: free, reflection at the outer boundaries of Δ, reflection at R, and transmission through R. Therefore it is convenient to represent the total stability matrix M of an orbit as the product of partial matrices that correspond to the different types of motion encountered by the orbit in the course of its history. The partial stability matrix $M^{(f)}$ for free (rectilinear) motion is given by

$$M^{(f)} = \begin{pmatrix} 1 & l \\ 0 & 1 \end{pmatrix}, \tag{10}$$

where $l=L/\sqrt{E-V}$ is the optical path length of the trajectory with L denoting its geometric length. The partial stability matrix $M^{(r)}$ for reflection is given by

$$M^{(r)} = \begin{pmatrix} -1 & 0 \\ 0 & -1 \end{pmatrix}. \tag{11}$$

The partial stability matrix $M^{(t)}$ for transmission through R can be calculated on the basis of simple geometrical considerations. An initial displacement in configuration space dX is mapped into the final displacement dX' after the transmis-

TABLE III. Analytical expressions (second column) for the free-motion part (characterized by its symbol listed in the first column) of the TSB Poincaré mapping.

Alphabet	x', β'
S,T	$x' = -[x\ \csc(2\alpha-\beta)\sin(\beta)],\ x\in(0,1)$ $\beta' = 2\alpha-\beta+\pi$ $\beta\in\left(\frac{\pi}{2}-\arctan\{[-x+\cos(2\alpha)]\csc(2\alpha)\},\pi\right)$
SP,TQ	$x' = 2+x\ \csc(2\alpha-\beta)\sin(\beta),\ x\in(0,1)$ $\beta' = -2\alpha+\beta$ $\beta\in\left(\frac{\pi}{2}-\arctan\left\{\frac{1}{2}[-x+2\cos(2\alpha)]\csc(2\alpha)\right\},\right.$ $\left.\frac{\pi}{2}-\arctan\{[-x+\cos(2\alpha)]\csc(2\alpha)\}\right)$
SPS,TQT	$x' = \csc(4a-\beta)[2\sin(2\alpha-\beta)+x\sin(\beta)],$ $x\in[0,2\csc(3\alpha)\sin(\alpha)]$ $\beta' = 4\alpha-\beta$ $\beta\in\left(\frac{\pi}{2}-\arctan[(1-x)\cot(\alpha)],\right.$ $\left.\frac{\pi}{2}-\arctan\left\{\frac{1}{2}[-x+2\cos(2\alpha)]\csc(2\alpha)\right\}\right)$
PSP,QTQ	$x' = 2-(2+x)\csc(2\alpha+\beta)\sin(\beta),\ x\in[2-\sec(2\alpha),1]$ $\beta' = -2\alpha-\beta+\pi$ $\beta\in\left\{\frac{\pi}{2}+\arctan[\cot(2\alpha)-(2-x)\csc(2\alpha)],\right.$ $\left.\frac{\pi}{2}-\arctan[(1-x)\cot(\alpha)]\right\}$
PS,QT	$x' = (2-x)\csc(2\alpha+\beta)\sin(\beta), x\in(0,1)$ $\beta' = 2\alpha+\beta$ $\beta\in\left\{0,\frac{\pi}{2}+\arctan[\cot(2\alpha)-(2-x)\csc(2\alpha)]\right\}$

sion through R [see Fig. 8(a)]. Using Snell's law (7) it follows that $dX' = g(\beta,\kappa)dX$, where we defined

$$g(\beta,\kappa) = \frac{\sqrt{\kappa^2-\cos^2(\beta)}}{\kappa\sin(\beta)}. \tag{12}$$

An initial displacement in momentum space dP is mapped into the final displacement dP' after the transmission through R [see Fig. 8(b)]. With $dp_x = dp_x'$ it follows that $dP' = dP/g(\beta,\kappa)$. The off-diagonal matrix elements are zero. This, too, can be seen in Fig. 8: An initial displacement in configuration space gives $dP' = 0$ and an initial displacement in momentum space gives $dX' = 0$. Thus the partial stability matrix for transmission from Δ_u to Δ_l is

$$M^{(t)} = \begin{pmatrix} g(\beta,\kappa) & 0 \\ 0 & 1/g(\beta,\kappa) \end{pmatrix}. \tag{13}$$

The partial stability matrix for transmission from Δ_l to Δ_u is $M^{(t)^{-1}}$. The partial stability matrix $M^{(\mathrm{ir})}$ for internal reflection at R is given by $M^{(\mathrm{ir})} = M^{(r)}$. The global stability matrix M for an orbit Ω is now easily constructed. Suppose Ω crosses the RS boundary m times. Denote by $M_i^{(f)}$ the free-motion partial stability matrix of Ω between transmissions i and $i+1$. Then

$$M = (-1)^B M_m^{(f)} M_m^{(t)} \cdots M_2^{(f)} M_2^{(t)} M_1^{(f)} M_1^{(t)^{-1}}, \tag{14}$$

where B is the total number of bounces of Ω including the bounces off R. Multiplying matrices we see that Eq. (14) has the structure

$$M = \begin{pmatrix} \Lambda & \star \\ 0 & 1/\Lambda \end{pmatrix}, \tag{15}$$

where Λ and $\star$ are real numbers. For two successive crossings with angles β_1 and β_2 one can show easily that

$$\Lambda = g(\beta_1,\kappa)/g(\beta_2,\kappa). \tag{16}$$

Because of the structure of Eq. (15) the eigenvalues of M are real and given by Λ and $1/\Lambda$. Thus, the periodic orbits of a polygonal RS billiard are either marginally stable or unstable. Marginally stable orbits may occur in families (for example, the family of orbits $B1$ in Fig. 5) or are isolated

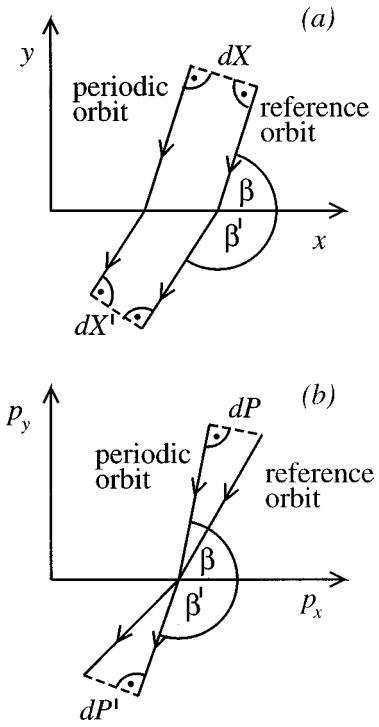

FIG. 8. Geometrical construction for the calculation of the partial stability matrix for the transmission through R (a) for the calculation of the first diagonal matrix element and (b) for the second diagonal matrix element.

(for example, the isolated orbit $C1$ in Fig. 5). Generally, marginally stable as well as unstable periodic orbits occur. Only in very special polygonal RS billiards do we not find truly unstable periodic orbits. An example is a rectangular step billiard with R as shown in Fig. 9: any trajectory that starts at R with an angle β_1 will cross R again with an angle β_2 where $\sin(\beta_1)=\sin(\beta_2)$. Therefore, according to Eq. (16) the modulus of the diagonal elements of M is equal to 1 and all periodic orbits are marginally stable. Because of the presence of truly unstable periodic orbits in the general case, we conjecture that generically polygonal RS billiards are ergodic. This conjecture is supported by the results of Sec. II F (see Fig. 7). Additional numerical evidence is presented in Sec. II H.

A second consequence of the structure of Eq. (15) is the absence of caustics. In quantum mechanics caustics are connected with the appearence of Maslov phases. Because of the zero in one of the off-diagonal elements of M together with the requirement that the determinant of M has to be 1, none of the diagonal elements of M can ever be zero. Thus we have no caustics in our system.

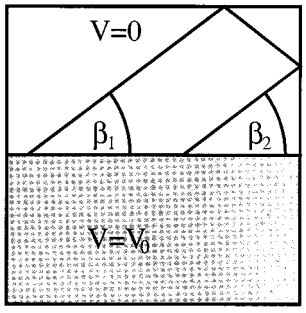

FIG. 9. A rectangular step billiard. Because of the right angles (corner cubes) formed by the boundaries of the billiard only marginally stable orbits exist.

H. Ergodicity and mixing

In this section we present numerical evidence for our conjecture that TSBs, generally, are ergodic, sensitive, and mixing. We checked ergodicity for $\mathrm{TSB}_0(0.51)$ at $E=1$ by dividing its phase space into cells of size $\Delta x=\Delta p_x=1/n$, $n=40,50,70$. We then performed the following numerical experiment. We started a trajectory at $x^{(0)}=0.3$, $p_x^{(0)}=0.1$ and mapped it foward in time. In every one of the three cases, i.e., $n=40$, 50, and 70, the trajectory visits all cells after N_n applications of the Poincaré mapping. We found $N_{40}=40\,770$, $N_{50}=111\,045$, and $N_{70}=206\,927$. Thus, within the limits of our check, $\mathrm{TSB}_0(0.51)$ is ergodic.

A dynamical system is sensitive if (except for a set of measure zero) two trajectories started anywhere in phase space within a distance ϵ will exceed a distance δ (smaller than the system dimensions) in finite time [12]. A first indication of sensitivity is our observation that numerical accuracy is completely lost along typical orbits over a time scale of several hundred Poincaré mappings. More directly we did the following numerical experiment. We defined 110 reference trajectories with initial conditions $x_{jk}^{(0)}=j/11$, $p_{xjk}^{(0)}=k/(6\sqrt{2})$, $j=1,\ldots,10$, $k=-5,\ldots,5$. For each one of the reference trajectories we defined a close-by trajectory $x_{jk}'^{(0)}=x_{jk}^{(0)}$, $p_{xjk}^{(0)}=p_{xjk}^{(0)}+\epsilon$ with $\epsilon=10^{-8}$. The distance between close-by trajectories and reference trajectories was computed according to $d_{jk}(N)=[(x_{jk}'^{(N)}-x_{jk}^{(N)})^2+(p_{xjk}'^{(N)}-p_{xjk}^{(N)})^2]^{1/2}$, where N is the number of applications of Poincaré mappings. We found that for all j,k the distance $d_{jk}(N)$ exceeded $\delta=0.1$ after less than $N=30\,000$ applications of the Poincaré mapping. Thus, with respect to $\epsilon=10^{-8}$, $\delta=0.1$ and the specific trajectories investigated TSB_0 is sensitive.

Further evidence for the sensitivity of TSBs derives from the probability distributions of the matrix elements of the stability matrix M. Let us denote by $M^{(N)}$ the stability matrix (15) of a typical phase-space orbit of length N. Since for TSBs the diagonal elements of $M^{(N)}$ are its eigenvalues, the probability distribution of the diagonal elements is a direct indication of the sensitivity of the associated TSB. According to the structure (15) of $M^{(N)}$ it is sufficient to compute the probability distribution $P(\lambda)$ of $\lambda=\ln(\Lambda^{(N)})$. The result is shown in Fig. 10 for $N=100$. $P(\lambda)$ is symmetric around $\lambda=0$. This means that the global Lyapunov exponent is zero. We checked this statement directly by computing the global Lyapunov exponent with the help of several long trajectories. Thus, the KS entropy of TSBs is zero. The spike of $P(\lambda)$ at $\lambda=0$ is due to the presence of marginally stable orbits. As mentioned already in Sec. II F (see also Fig. 7) long trajectories get ''stuck'' in the vicinity of marginally stable orbits giving a large weight to $|\Lambda|=1$. The most important observation in Fig. 10 is the bell shape of the distribution. This means that Λ can get arbitrarily large with nonzero probability, which supports the sensitivity claim. Since there is no

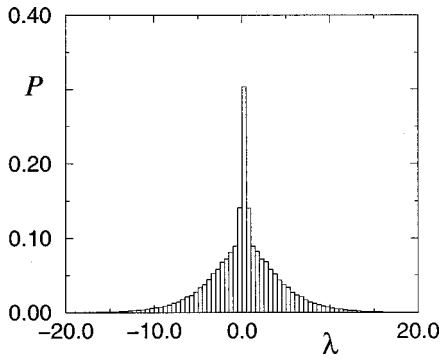

FIG. 10. Probability distribution $P(\lambda)$ of the logarithm of the stability $\lambda=\ln(\Lambda^{(N)})$ computed from long TSB_0 orbits for $N=100$.

reason to doubt that periodic orbits are dense in the TSB phase space, TSBs are chaotic according to Devaney's criteria of chaos [12].

Furthermore we have numerical evidence that TSBs are mixing. A dynamical system is mixing if in the limit $n\to\infty$ we have

$$\rho(\mathcal{P}_n(A)\cap B)=\rho(A)\rho(B). \tag{17}$$

Here, $\mathcal{P}_n$ is the n-times iterated Poincaré mapping $\mathcal{P}$ and ρ is the invariant measure on the TSB phase space. We checked Eq. (17) with the following numerical experiment with $TSB_0(1/2)$ at $E=1$ and $n=100$. We defined the phase-space set A as the rectangle $0.4\leqslant x\leqslant 0.5$, $0.1\leqslant p_x\leqslant 0.2$ and set $B=A$. Next we ran 20 trajectories started at $x_j^{(0)}=j/200$, $p_{xj}^{(0)}=j/400$, $j=1,\ldots,20$ over $N=10^7$ applications of $\mathcal{P}$ each. For each one of the 20 trajectories we checked its position in phase space in steps of 100 Poincaré mappings, which results in $M=20\times N/100$ check points. We found that $M_1=13\,808$ phase-space points out of M fell into A. This way we obtained an approximation $r(A)=M_1/M=6.9\times10^{-3}$ to the measure $\rho(A)$. Next we used the M_1 phase-space points that fell into A as starting conditions and mapped them forward $n=100$ steps. We found that this time $M_2=106$ points fell into A. This way we obtain the ratio $s=M_2/M_1=7.7\times10^{-3}$ as an approximation to $\rho(\mathcal{P}_n(A)\cap A)/\rho(A)$. The two ratios are close, supporting our conjecture that generally TSBs are mixing.

III. QUANTUM MECHANICS

In this section we investigate the quantum mechanics of $\mathcal{T}$. We will see that the morphology of TSB wave functions is very different from the appearance of split circle wave functions presented in [4]. In Sec. III A we describe our numerical method. It is different from the method used in [4], though both rest on direct diagonalization. Although inefficient, direct diagonalization is the method of choice if both energy levels and wave functions are desired. In Sec. III B we present some typical TSB wave functions. The RS correction of the Weyl formula, derived and tested in the context of a separable system in [2], is tested in Sec. III C in the context of a nonseparable chaotic TSB. The signatures of Newtonian and non-Newtonian TSB orbits are identified in Sec. III D in the Fourier transform of scaled TSB energy levels.

A. Numerical method

The stationary Schrödinger equation for TSBs is given by

$$\hat{H}\psi_n(x,y)=E_n\psi_n(x,y), \tag{18}$$

where

$$\hat{H}=\left[-\frac{d^2}{dx^2}-\frac{d^2}{dy^2}\right]+V(x,y). \tag{19}$$

The potential $V(x,y)$ is defined in Eq. (2). We solve Eq. (18) in three steps. (i) We solve for the stationary eigenfunctions

$$\left[-\frac{d^2}{dx^2}-\frac{d^2}{dy^2}\right]\phi_i(x,y)=E_i\phi_i(x,y) \tag{20}$$

of an auxiliary problem defined as an isosceles triangle with $\alpha=\pi/4$ and Dirichlet boundary conditions [13]. (ii) With the help of a simple scaling in the y direction we define a basis set $\{\tilde{\phi}_k(x,y)\}$ on Δ given by

$$\tilde{\phi}_k(x,y)=\frac{1}{\sqrt{\tan\,\alpha}}\,\phi_k(x,y/\tan\,\alpha). \tag{21}$$

The set (21) is orthonormal on Δ according to

$$\int_\Delta\int dxdy\,\tilde{\phi}_k(x,y)\tilde{\phi}_l(x,y)=\delta_{kl}. \tag{22}$$

(iii) We expand ψ_n in the $\tilde{\phi}_i$ basis:

$$\psi_n(x,y)=\sum_{i=1}^{N}a_{ni}\tilde{\phi}_i(x,y). \tag{23}$$

(iv) We diagonalize $\tilde{H}$ in the basis $\{\tilde{\phi}_k(x,y)\}$ and obtain E_n and $\psi_n(x,y)$. The advantage of this method is that it is capable of dealing with the boundary condition in a trivial way. The disadvantage is that this method attempts to expand the step potential of the TSB, a nondifferentiable function on R, into a set of smooth functions. Although possible in principle, the convergence is slow. Nevertheless we use this method because the advantage of easy handling by far outweighs the disadvantage of slow convergence.

B. Wave functions and spectral statistics

In order to identify classical orbits in the Fourier spectrum of the density of states, it is useful to solve the scaled Schrödinger equation [4,14], i.e., to solve the Schrödinger equation for constant η. Wave functions for the scaled Schrödinger equation for TSB_0 and $\eta=1/2$ are shown as gray-scale plots in Fig. 11. The numbers adjacent to the plots correspond to the quantum numbers n of the wave functions. Apart from the difference in the local wave number that trivially reflects the two different values of the potential in Δ_u and Δ_l, respectively, all wave functions in Fig. 11 are featureless and homogeneously distributed over the interior of TSB_0. This means that TSB wave functions behave very differently from

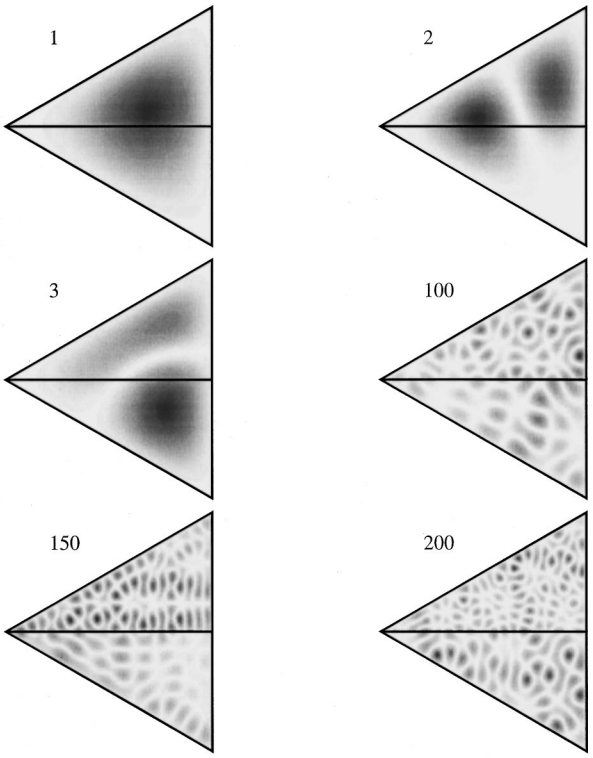

FIG. 11. Gallery of wave functions for the scaled TSB_0 with $\eta=1/2$. The labels refer to the quantum number n of the wave function. Plotted is $|\psi_n(x,y)|$. The darker the shade of grey, the larger $|\psi_n(x,y)|$.

the wave functions shown in [4] for the circular RS billiard. In [4] even at higher energies, most of the wave functions show regular structure.

An interesting feature in the TSB wave functions appears at higher energies: the emergence of short-range correlations in the form of scarlets [15,16]. Scarlets appear in random wave functions of fixed energy [15] and support our conjecture that TSB wave functions are ''ergodic.'' Scarlets also appear in the high energy wave functions of hyberbolic billiards [17], which means that TSBs, to a certain extent, mimic hyperbolic systems. In this context we computed the nearest neighbor spacing statistics for TSB_0. We found it to be Wigner-type. While this result is consistent with the conjectured chaos of TSBs, it cannot be cited as a further argument to support the claim of chaos, since it was shown [18] that pseudointegrable triangles also exhibit Wigner-type statistics. We checked this result by computing the nearest neighbor statistics for $TSB_0(0)$, a pseudointegrable rational triangle. After symmetry reduction we found its nearest neighbor spacing statistics to be Wigner-type as expected.

For $E_n>V_0$ wave functions for the unscaled problem look very similar to the wave functions of the scaled problem shown in Fig. 11. The only noteworthy exception we found is the wave function $n=61$ of $TSB_0(3000)$. It is shown in Fig. 12. It may be interpreted as a scar corresponding to the NN orbit $d1$ of Fig. 6. So far we have not seen regular sequences of NN scars.

C. Test of the RS correction

The smoothed density of states for TSBs ($E>0$) with Dirichlet boundary conditions is given by the Weyl formula [3]

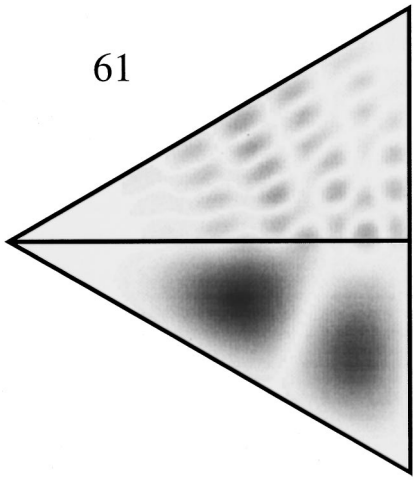

FIG. 12. The wave function $n=61$ (unscaled) for $TSB_0(3000)$. It scars the non-Newtonian orbit $d1$ of Fig. 6.

$$\overline{\mathcal{N}}(E,V_0)=\frac{A}{8\pi}\left[E+(E-V_0)\,\theta(E-V_0)\right]-\frac{L}{4\pi}\left[\sqrt{E}+\sqrt{E-V_0}\,\theta(E-V_0)\right]+R\sqrt{V_0}\,\overline{\nu_{\mathrm{RS}}}(z)+(\text{corrections}),\qquad(24)$$

where $\theta(x)$ is Heaviside's step function, A is the area of the TSB, $L=S+P$ and $\overline{\nu_{\mathrm{RS}}}(z)$ is the RS correction derived in [2]. The variable z is $z=1/\eta$. Additional corrections are summarized in the term ''corrections.'' They are expected to be small. In [2] the agreement of the analytical prediction for $\overline{\nu_{\mathrm{RS}}}$ with numerical data was demonstrated for a rectangular RS billiard with mixed boundary conditions. In [2] the RS boundary is identical to one of the symmetry axes of the billiard as shown in Fig. 9. This system consists only of marginally stable orbits as demonstrated in Sec. II G. The formula for $\overline{\nu_{\mathrm{RS}}}$ was not yet tested for a chaotic system. In Fig. 13 we plot $\overline{\nu_{\mathrm{RS}}}$ as a function of $z=1/\eta$. The smooth line is the analytical RS correction, the jagged line is the numerical result for $\overline{\nu_{\mathrm{RS}}}$ computed for $TSB_0(6000)$. The agreement is very good. There is a small systematic deviation for large z. Since large z corresponds to high energy, we attribute this deviation to a loss of accuracy in the computa-

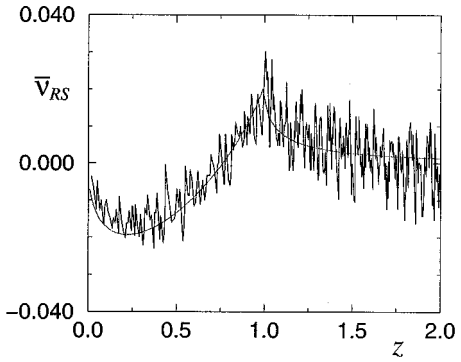

FIG. 13. Test of the RS correction. The smooth line is the analytical result computed in [2]. The jagged line is the numerical result obtained for $TSB_0(6000)$ with Dirichlet boundary conditions.

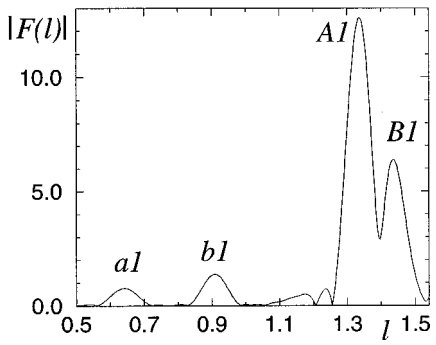

FIG. 14. Fourier transform of the scaled energy spectrum of TSB_0 with $\eta=1/2$.

tion of high lying energy eigenvalues. Thus, the analytically derived RS correction passes a first test in the context of a chaotic system.

D. Fourier transformation

The Gutzwiller trace formula [3] gives the fluctuating part of the level density in terms of classical periodic orbits of a two-dimensional system. The Gutzwiller formula has been extended to systems with ray splitting [1]:

$$\widetilde{\rho}_{sc}(E)=\mathrm{Im}\left\{\frac{1}{i\hbar}\sum_j \frac{A_j^{1/2}T_j}{|\Lambda_j|^{1/2}|1-1/\Lambda_j|}\times\exp\{i[(S_j/\hbar)+\delta_j]\}\right\}. \tag{25}$$

The summation is over all periodic orbits, Newtonian and non-Newtonian, S_j is the action, T_j the period, and Λ_j is defined in Eq. (15). Since TSBs do not have any caustics (see Sec. II G), Maslov phases are absent and only trivial phases due to reflections contribute to δ_j. The quantity A_j is given by

$$A_j=\left[\prod_{i=1}^{\varrho_j}|r_{ij}|^2\right]\left[\prod_{k=1}^{\tau_j}(1-|r_{kj}|^2)\right], \tag{26}$$

where ϱ_j (τ_j) are the number of reflections (transmissions) encountered by the periodic orbit j and r_{ij} is the reflection coefficient at the ith reflection. In order to identify periodic orbits in the level density $\widetilde{\rho}(E)$ of TSBs we Fourier transform the quantum mechanical $\widetilde{\rho}_{\mathrm{qm}}(\eta,E)$ in the following way:

$$F(l)=\int \widetilde{\rho}_{\mathrm{qm}}(E)\exp(-il\sqrt{E})dE. \tag{27}$$

Because of the semiclassical formula (25) we expect peaks at the scaled action l of classical orbits. We Fourier transform the scaled density of states because for constant η the quantities A_j are independent of E. In Fig. 14 we show $|F(l)|$ for TSB_0 in the range $1/2<l<3/2$ for $\eta=1/2$. The resulting peaks in $F(l)$ can be assigned to periodic orbits using Table II: The two small peaks are due to the NN orbits $a1$ and $b1$ (see Fig. 6). The two large peaks are due to the Newtonian orbits $A1$ and $B1$ (see Fig. 5). It is interesting to note that the orbit $B1$ produces a peak in $F(l)$ at all, since for $\eta=1/2$ it does not correspond to a periodic orbit. However, for $\eta=1/2$ it is very close to periodic, and leaves its mark as a distinct peak in Fig. 14. The action of the approximately closed orbit $B1$ at $\eta=1/2$ differs from the value listed in Table II. For $\eta=1/2$ it shifts to a value very close to the position of the peak marked ''$B1$'' in Fig. 14.

IV. SUMMARY AND CONCLUSIONS

In this paper we presented a detailed classical and quantum mechanical analysis of a class $\mathcal{T}$ of triangular step billiards. We showed analytically the absence of elliptic islands in the TSB phase space; i.e., TSBs do not possess any stable orbits. There is at most a set of marginally stable orbits of measure zero in phase space. We also presented numerical indications that TSBs are ergodic, sensitive, and mixing. Thus, within the limits of our numerical tests, TSBs are chaotic. The KS entropy of TSBs was found to be zero. In the quantum mechanical part of this paper we presented a simple method for the solution of the TSB Schrödinger equation. Using this method we computed quantum energy levels and quantum wave functions for the scaled and unscaled TSB problems. The wave functions computed are distributed homogeneously over the surface of the billiard. This is in marked contrast to the behavior of split circle wave functions which show a fascinating variety of regular structures and scars. Thus TSB wave functions are very close to ''ergodic,'' a feature expected for a completely chaotic system. We also tested the RS correction to the Weyl formula in the context of a chaotic system. Within the numerical accuracy the computed RS correction is consistent with the analytical prediction. Isolated non-Newtonian TSB orbits were identified in the Fourier transform of the scaled density of states. As demonstrated in Sec. II and in Appendix A, many features of TSBs can be computed analytically. Compared to the split circle billiard defined in [4] the particular strength of TSBs rests in their much simpler phase-space structure and easy access to its analytical properties. In analogy to the experiments of Ref. [6] TSB's can be realized experimentally with the help of a triangularly shaped thin microwave cavity partially filled with teflon. We hope that such experiments will soon be performed.

ACKNOWLEDGMENTS

The authors thank Kai T. Hansen, Olaf Frank, Debabrata Biswas, and Predrag Cvitanović for helpful discussions. We gratefully acknowledge financial support by the Deutsche Forschungsgemeinschaft.

APPENDIX A

Consider the periodic orbit shown in Fig. 15. The orbit is launched at ξ with momentum p_ξ into Δ_u. The task is to compute ξ and p_ξ as well as the action of the orbit explicitly as a function of γ and V_0. The momentum p_ξ can be computed immediately. With $\varphi'=\pi/2-\gamma$, Snell's law of refraction (7) relates φ to γ. We obtain

$$p_\xi=\sin(\varphi)=\kappa\cos(\gamma). \tag{A1}$$

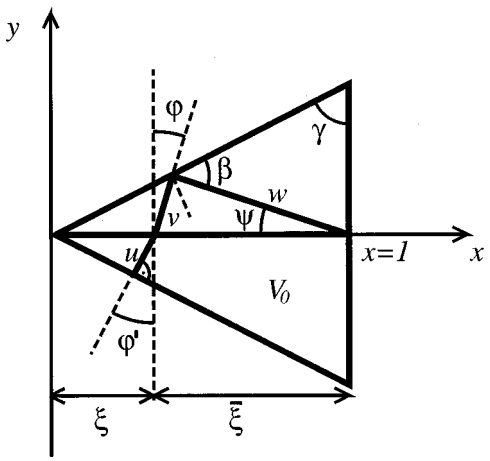

FIG. 15. Sketch of the orbit $C1$.

Next we use the law of sines in the triangle spanned by w, γ, and β to obtain

$$w=\cos(\gamma)[\sin^2(\gamma)\sqrt{1+V_0\ \cot^2(\gamma)}-\kappa\ \cos^2(\gamma)]^{-1}. \tag{A2}$$

We apply the law of sines to the triangle spanned by w and ξ. With $\bar{\xi}=1-\xi$ we obtain

$$\xi=1-2\cos^2(\gamma)\left[1+\frac{\kappa}{\sqrt{1+V_0\ \cot^2(\gamma)}}\right]. \tag{A3}$$

In order to compute the action of the periodic orbit shown in Fig. 15 we also need u and v. With w and ξ known explicitly, we apply the law of sines to the triangle spanned by ξ and v and obtain

$$v=w\xi. \tag{A4}$$

The computation of u is trivial:

$$u=\xi\ \cos(\gamma). \tag{A5}$$

The action of the periodic orbit is now given explicitly by

$$S=2(\kappa u+v+w). \tag{A6}$$

[1] L. Couchman, E. Ott, and T. M. Antonsen, Jr., Phys. Rev. A **46**, 6193 (1992).
[2] R. E. Prange, E. Ott, T. M. Antonsen, Jr., B. Georgeot, and R. Blümel, Phys. Rev. E **53**, 207 (1996).
[3] M. C. Gutzwiller, *Chaos in Classical and Quantum Mechanics* (Springer, New York, 1990).
[4] R. Blümel, T. M. Antonsen, B. Georgeot, E. Ott, and R. E. Prange, Phys. Rev. Lett. **76**, 2476 (1996); Phys. Rev. E **53**, 3284 (1996).
[5] R. Blümel and A. Kohler, Phys. Bl. **52**, 1243 (1996).
[6] L. Sirko, P. M. Koch, and R. Blümel, Phys. Rev. Lett. **78**, 2940 (1997).
[7] P. J. Richens and M. V. Berry, Physica D **2**, 495 (1981).
[8] K. T. Hansen, Phys. Rev. E **52**, 2388 (1995).
[9] K. T. Hansen and A. Kohler, Phys. Rev. E **54**, 6214 (1996).
[10] B. Eckhardt and D. Wintgen, J. Phys. A **24**, 4335 (1991).
[11] M. Sieber and F. Steiner, Physica D **44**, 248 (1990).
[12] R. L. Devaney, *A First Course in Chaotic Dynamical Systems* (Addison-Wesley, Reading, MA, 1992).
[13] F. E. Borgnis and C. H. Papas, in *Handbuch der Physik*, Vol. XVI, edited by S. Flügge (Springer-Verlag, Berlin, 1958), pp. 285–422.
[14] H. Friedrich and D. Wintgen, Phys. Rep. **183**, 37 (1989).
[15] P. O'Connor, J. Gehlen, and E. J. Heller, Phys. Rev. Lett. **58**, 1296 (1987).
[16] R. Blümel, I. H. Davidson, W. P. Reinhardt, H. Lin, and M. Sharnoff, Phys. Rev. A **45**, 2641 (1992).
[17] R. Aurich and F. Steiner, Physica D **48**, 445 (1991); **64**, 185 (1993).
[18] M. V. Berry and M. Wilkinson, Proc. R. Soc. London, Ser. A **392**, 15 (1984).